Impedance and AC conductivity study of nano crystalline, fine grained multiferroic bismuth ferrite (BiFeO$_3$), synthesized by microwave sintering

Jayant Kolte, Paresh H. Salame, A. S. Daryapurkar, et al.

Impedance and AC conductivity study of nano crystalline, fine grained multiferroic bismuth ferrite (BiFeO$_3$), synthesized by microwave sintering

Jayant Kolte,[1] Paresh H. Salame,[2] A. S. Daryapurkar,[1] and P. Gopalan[1]
[1]*Dept. of Metallurgical Engineering & Materials Science, Indian Institute of Technology Bombay, India*
[2]*Dept. of Applied Physics, Laxminarayan Institute of Technology, RTM Nagpur University, India*

In this paper, major reduction in sintering time, temperautre and significant improvement over final density of sitnered sample is reported for the microwave sintered nanocrystalline BiFeO$_3$ (BFO) ceramic. Also, different sintering time and temperatures have been used to tailor the grain size and the final density of the resulting BFO ceramics synthesized from phase pure BFO nanoparticles ($\bar{d} \approx 10\,nm$). Microwave sintering resulted in reducing the sintering time substantially (by 1h), and has resulted in submicron sized grains and high resistivity $\sim$ 1.8 GΩ-cm. The AC conductivity is seen to follow the Jonscher's power law behavior, suggesting correlated barrier hopping (CBH) mechanism in the sample. The role of oxygen vacancies at high temperature, due to volatility of bismuth, in dielectric and conductivity behavior is also discussed. Further, the sample displayed dielectric anomaly near magnetic transition temperature ($\sim$180 °C) indicating bearing of magnetic moments on the dielectric properties. Using Impedance Spectroscopy (IS) we have established, the electrical heterogeneity of the ceramic BFO reavealing semiconducting nature of grains and insulating nature of grain boundary. This, formation of network of insulating grain boundaries and semiconducting grains could lead to formation of internal barrier layer capacitance (IBLC) leading to high dielectric constant in microwave sintered BFO. © *2015 Author(s). All article content, except where otherwise noted, is licensed under a Creative Commons Attribution 3.0 Unported License.* [http://dx.doi.org/10.1063/1.4931818]

I. INTRODUCTION

Multiferroic materials have been widely investigated in the past decade due to simultaneous exhibition of multiple ferroic properties such as ferroelectricity, ferromagnetism and ferroelasticity. BiFeO$_3$ (BFO) is the most widely investigated material possibly due to the exhibition of multiferroic behavior at room temperature.[1] BFO has high Curie temperature (T$_C$ $\sim$ 830 °C) and high antiferromagnetic transition temperature (T$_N$ $\sim$ 370 °C).[2,3] BFO have also been investigated for various potential applications such as sensors, transducers, memory devices, actuators, magnetoelectrics, spintronic, photovoltaic devices *etc*.[1,4–7] However, there are still a few challenges in BFO that needs to overcome, such as a metastable phase, high leakage current, and high coercive field.[8–10] Also, during synthesis and sintering process, BFO may form secondary phases such as Bi$_2$Fe$_4$O$_9$, Bi$_{25}$FeO$_{39}$ and Bi$_2$O$_3$ due to Bismuth volatility.[8,11–13] These problems have been eliminated using careful synthesis of BFO by using PVA sol gel method.[14] These problems can be further reduce if we can minimize the sintering temperature and time; microwave sintering is one such technique.

In polycrystalline ceramics, the electrical properties are mostly influenced by presence of grains and grain boundaries.[15,16] Dielectric behavior of ceramics may show considerable variation depending on nature of the grains and grain boundaries as well as overall morphology of microstructure.[17–22] In microwave heating, electromagnetic waves interact substantially with the ceramics, stimulating volumetric heating, which subsequently enhance densification, microstructure homogeneity, leading to reduction in sintering temperature.[23–25] Many ferroelectric materials have

been synthesized by using microwave sintering method due to advantages such as, high heating rates of microwave sintering, prominently shortening of the processing time and temperature as compared to conventional sintering techniques.[23–29] Considering the plausible reduction in sintering time and temperature, probability of bismuth loss could be minimized, which in turn could prove advantageous to the electrical properties of $BiFeO_3$. However, barring few[25,27,28] which have shown significant reduction in leakage current, there is hardly any literature on microwave sintered BFO and especially on the impedance spectroscopy (IS) of the microwave sintered BFO ceramic.

In this paper, effect of microwave sintering on the microstructure and various electrical properties *viz.* dielectric, impedance and AC conductivity of phase pure BFO has been studied. We have revealed through impedance spectroscopy that electrical microstructure of microwave sintered $BiFeO_3$ ceramics is electrically heterogeneous with semiconducting grains and insulating grain boundaries; this could lead to internal barrier layer capacitance (IBLC) in the sample which might be ultimately held responsible for high ε_r' in microwave sintered, fine grained, nanocrystalline $BiFeO_3$ apart from other extrinsic effects.

II. EXPERIMENTAL

$BiFeO_3$ nanopowders were synthesized by using PVA sol gel method with monodispersed particle size ($\bar{d} \approx 10$ nm).[14] The phase purity of the powder was examined using X-ray diffractometer (PANalytical X'pert PRO) in the scanning range from 20° to 90° at scan rate of 0.01°/10 sec. The lattice parameters of these powders were refined using Fullprof Rietveld refinement software.[30] Subsequently, the phase formed BFO powder was pressed uniaxially into 10 mm diameter pellets. Further, these green pellets were sintered isothermally in a microwave furnace with a sacrificial powder of the same composition. The pellets were kept at different sintering temperature *viz.* 750°C and 800°C, for 1-2 hours at each selected temperature. The density of the pellets were calculated using Archimedes principle (ASTM no.: C 20-00). Surface morphology of sintered pellets were studied using scanning electron microscopy (JEOL JSM-7600F). For electrical characterization, the pellets were coated with silver paint and cured at 200°C for 2 hours. Impedance measurements were carried in the temperature of −50°C to 350°C using high resolution Alpha-A broadband dielectric spectrometer (Novocontrol GmbH, Aubachstr Germany) in the frequency range of 1 Hz to 1 MHz at $1V_{rms}$.

III. RESULT AND DISCUSSION

The X-ray diffraction pattern of BFO pellets sintered at 750 °C and 800 °C each for 1 and 2 h, is shown in Figure 1(a). It was confirmed from matching of the sample with standard JCPDS data that all samples have Rhombohedral crystal structure with R3c space group. All the BFO samples
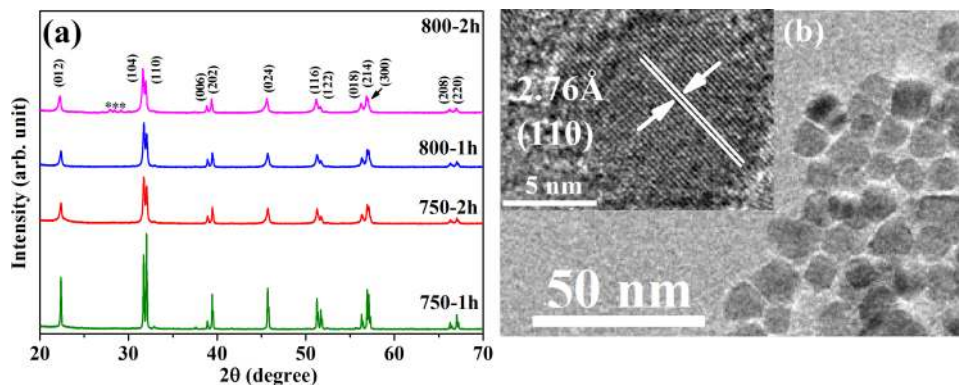

FIG. 1. (a) Powder X-ray diffraction pattern of $BiFeO_3$ ceramics, microwave sintered at different temperatures for the cycle of 1 and 2 hours. (Impurity phases in XRD pattern are indicated by *) (b) TEM micrograph of BFO powder synthesized by PVA sol gel method. (Inset shows the HRTEM image of 110 plane).

TABLE I. Rietveld refinement parameters of microwave sintered $BiFeO_3$ samples at various temperature and time, values in parenthesis indicates the uncertainty in lattice parameter computation in last digit.

Sintering temperature/Duration	$a = b$ (Å)	c (Å)	R_{wp}	R_{exp}	S (R_{wp}/R_{exp})	χ^2
750 °C/1h	5.576(1)	13.864(1)	16.9	10.21	1.65	2.74
750 °C/2h	5.575(2)	13.865(2)	21.2	12.25	1.73	3.01
800 °C/1h	5.577(3)	13.866(3)	19.8	12.09	1.63	2.69
800 °C/2h	5.573(1)	13.862(1)	22.2	11.99	1.85	3.41

exhibited phase purity except the sample sintered at 800 °C/2 h which have shown some minor peaks of impurity phase (indicated by *). The increase in sintering time at 800 °C lead to volatility of Bismuth and formation of various secondary phases.[8,11–13]

The lattice parameters of all the samples were obtained by refining the data using Fullprof software[30] and is presented in Table I. No significant change in lattice parameter is observed for samples sintered in various sintering condition. Bismuth ferrite nanoparticles synthesized via PVA sol gel method are shown in Figure 1(b). The particles are well dispersed and the average size is ~10 nm. Inset of Figure 1(b) shows the High resolution TEM image of single particle showing (110) orientation.

For $BiFeO_3$ green pellets consolidate using microwave sintering, the sintering conditions were so chosen that we can get the samples with highest apparent density. SEM images of BFO samples synthesized by microwave sintering at various temperatures and time is shown in Figure 2. The average grain size of the sample sintered at 750 °C/1h (Figure 2(a)) is found to be submicron sized (≤ 338 nm). The sample appears to be in the initial stage of the sintering process, and neck formation is observed in the sample. As the sintering time increases to 2 hours (Figure 2(b)), the grain size is also found to increase to 365 nm. Samples sintered at 800 °C for 1 hour, and 2 hours are shown in Figure 2(c) and 2(d) respectively, wherein sample reveled complete grain growth. The sample show uniform grain distribution having grain size (~ 850 nm) for sample sintered at 800 °C for 1 hour.
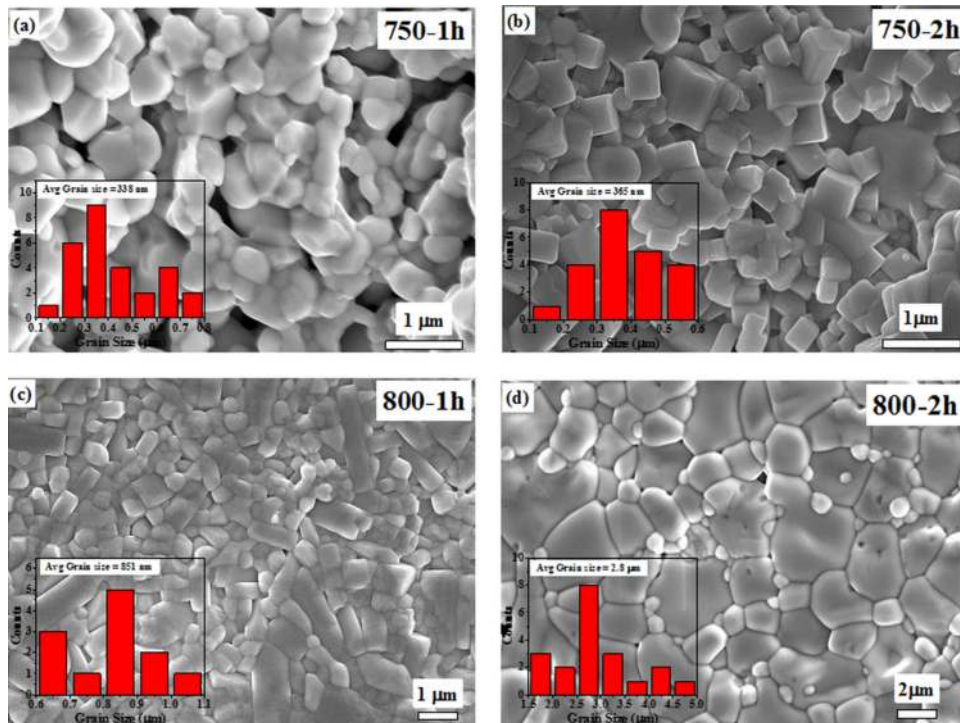

FIG. 2. Scanning electron microscopy images of BFO sample sintered at (a) 750 °C for one hour, (b) 750 °C for two hours, (c) 800 °C for one hour and (d) 800 °C for two hours.

As for the sample sintered for 2 hours, the grain distribution become dense with increase in average grain size of around 2.8 μm. The sample sintered at 800 °C for 1 hours is highly dense (> 95%) with uniform microstructure, with few elongated, rod shaped grains. The increase in sintering time (2 h at 800 °C) have given a way for grains to become coarser on account of finer grains at 800 °C/1h, and the microstructure is showing somewhat bimodal distribution of grains.

In several reports on ceramic BiFeO₃ so far, various mechanism were proposed for dielectric relaxation in BFO samples (*viz.* Hopping or Maxwell Wagner based) and were contested to base on processing conditions.[31–33] In all these reports, the grain-size/microstructure was considered an important factor in determining the overall electrical properties of the sample. In view of this, here also, we engineered the BFO ceramics in various grain sizes in anticipation of variation electrical properties; although all the microwave sintered samples exhibited some change in their dielec-tric/electrical properties, their overall trend, for all the samples, remained same. Various relaxation peaks and impedance behavior for all the samples followed the similar trend. Based on this, to explain the dielectric phenomenon in microwave sintered BFO only the sample sintered at 800°C/1h is chosen on account of its superior microstructure and improved density over other samples.

The frequency dispersion of various dielectric parameters at a few discrete sample temperatures is shown in Figure 3. A clear Maxwell-Wagner type relaxation process can be seen from the spectroscopic plots of ε_r' and tan δ, wherein, a step-like decrease in ε_r' can be seen to be accompanied by the corresponding relaxation peaks in tan δ. Further, this corresponding peak in tan δ can be seen shifting towards higher frequencies with increasing temperature, indicating Debye type thermally activated mechanism.[34] According to this mechanism whenever the hopping frequency of charge carriers matches with the applied frequency, a peak in tan δ is observed. This conductivity contri-bution due to hopping of charge carriers is evident from Figure 3(b), where ε_r'' can be seen varying with slope $(\Delta\varepsilon''/\Delta f)$ of −1 which indicate that ε_r'' is dominated by conductivity, $\sigma(\omega)$[35,36] and is given by the equation (1);

$$\varepsilon_r'' \approx (\sigma_{dc}/\varepsilon_0\omega) \tag{1}$$
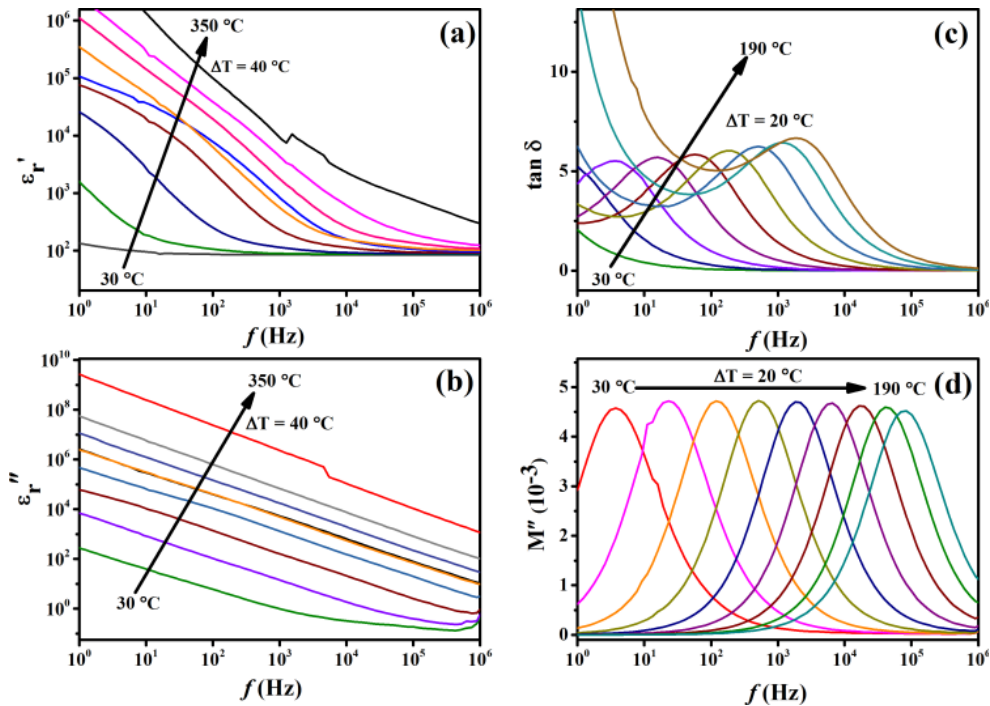

FIG. 3. (a) Frequency variation of the real part of dielectric constant (ε_r'), (b) imaginary part of dielectric constant (ε_r''), (c) tan δ and (d) imaginary part of modulus at a few discrete temperatures for microwave sintered BFO ceramic at 800°C/1h. (Figure 3(c) shows the peak in tan δ corresponding to relaxation peak in dielectric constant ε_r').
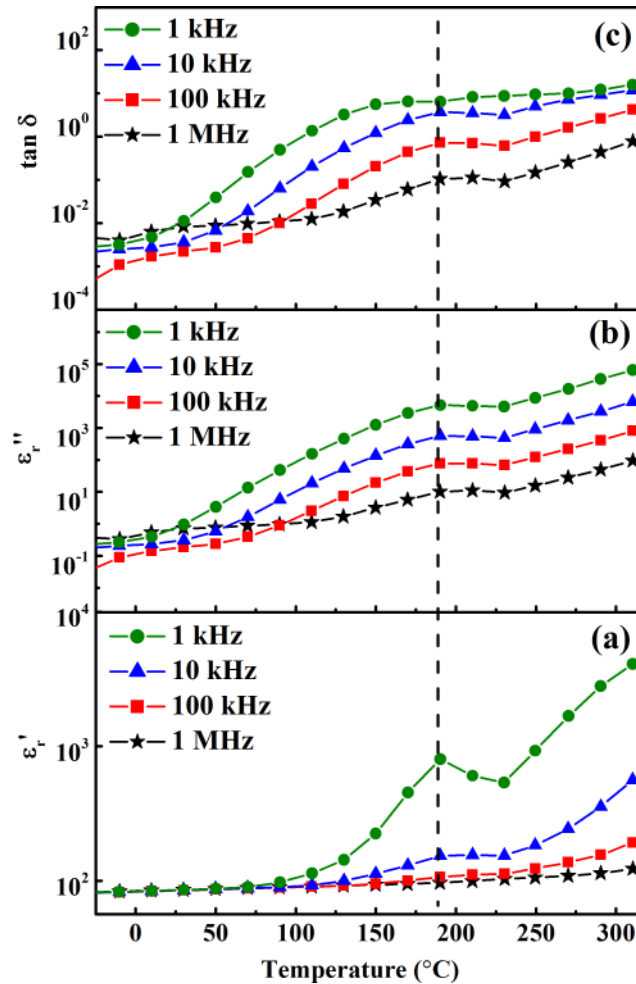
FIG. 4. Temperature dependence of (a) ε_r', (b) ε_r'' and (c) tanδ for microwave sintered BFO (800 °C/1hr) measured at a few selected frequencies. The relaxation peaks here are seen to be very close to the antiferromagnetic ordering temperature of BFO.

where, σ_{dc} is conductivity at the lowest measured frequency, ε_0 (8.85×10^{-12} Fm^{-1}) is the permittivity of the free space and ω (angular frequency) = $2\pi\nu$.

From the Figure 3(a), it is now evident that the Maxwell Wagner response, dipolar contribution due to hopping of charge carriers between the available states and space charge polarization (which can be seen for frequency < 100 Hz) are primarily responsible for the occurrence of high ε_r' (> 10^3) in the microwave sintered BFO ceramics. While the losses in the sample are due to conductivity ($\sigma(\omega)$) in the sample. Figure 3(d) shows the modulus spectroscopic plot versus frequency at temperatures from 30 °C to 190 °C. Peak in modulus spectra of microwave sintered BFO (Figure 3(d)) suggest the temperature dependent hopping mechanism. It also has strong temperature dependent peak frequency.

To see the temperature dependence of dielectric properties of the microwave sintered BFO, the dielectric constant (ε_r') at few selected frequencies is plotted in Figure 4(a). It is clearly observed that, as the temperature is increased the dielectric constant at all frequencies increases due to thermally activated charge carriers. The dielectric constant (ε_r') almost remains constant till 230 °C for frequencies > 10 kHz, then it starts to increase with temperature. Further, at 1 kHz and 10 kHz a broad relaxation peak is observed in between 175 °C to 200 °C. This relaxation in ε_r' is interestingly close to the magnetic transition temperature of BFO, indicating the magneto-electric coupling in BFO.[1,37,38] The Room temperature dielectric constant and dielectric loss was found to be ~85 and ~0.01 at 100 kHz respectively, which is higher than earlier reported BFO samples sintered
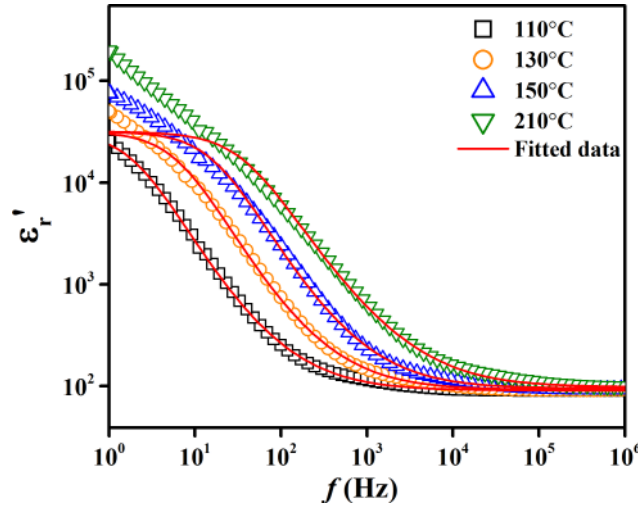
FIG. 5. Real part of the dielectric constant with frequency measured at selected temperatures; the red solid lines are fitted curves according to Cole–Cole equation.

conventionally[32,39–41] possibly due to space charges and grain boundary effects. It is also observed that, at lower temperature (< 50 °C), ε_r' becomes almost temperature independent for all frequencies, which can be attributed to static dielectric response[42]

To explore the nature of the dielectric relaxation in the BFO ceramics, the data of the dielectric spectra were fitted with the Cole–Cole equation[43] as shown in Figure 5,

$$\varepsilon^* = \varepsilon' - j\varepsilon'' = \varepsilon_\infty + \frac{(\varepsilon_s - \varepsilon_\infty)}{1 + (j\omega\tau)^{1-\alpha}} \tag{2}$$

Where, ε^* is the complex permittivity, ε_s and ε_∞ are the static and high frequency limits of dielectric permittivity. τ is the relaxation time, $\omega = 2\pi f$ is the angular frequency and α is the measure of the distribution of relaxation time and always lie in between 0 and 1.

According to Cole–Cole equation, the fitted parameters for microwave sintered BFO is shown in Table II. Due to space charge contributions at lower frequency, the Cole-Cole equation could not be fit to experimental data. It can be observed that the sample follows Debye type relaxation in the temperature ranges from 110 – 210 °C and also the relaxation time (τ) can be seen decreasing with temperature. It can be inferred that the relaxation process is thermally activated, as with increasing temperature the relaxation peaks can be seen shifting towards higher frequency side.

The spectroscopic plots of the real part of ac conductivity (σ_{ac}') at few discrete temperature is shown in Figure 6(a). As the temperature increases the AC conductivity increases due to thermally generated charge carriers. Further, the AC conductivity is seen to follow the Johnscher's power law given by,[44]

$$\sigma_{ac} = \sigma_{dc} + A\omega^n \tag{3}$$

TABLE II. Dielectric relaxation time (τ) and distribution of relaxation time (α) obtained as a function of temperature fitted by Cole–Cole equation. (Relaxation time decreases as a function of temperature).

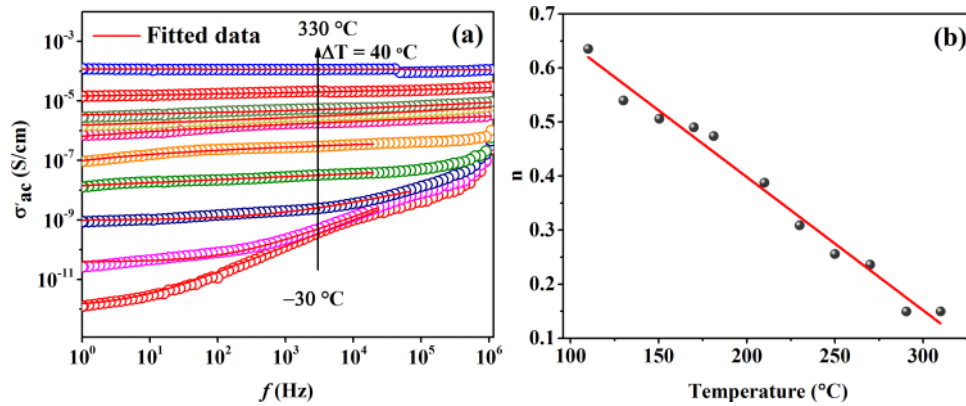| °C	τ	α
110	0.0802	0.8991
130	0.01195	0.9206
150	0.00645	0.9076
170	0.00229	0.9077
190	0.00129	0.8928
210	0.00702	0.8535
230	0.00436	0.893

FIG. 6. (a) AC conductivity study of BFO ceramics measured at different temperatures (red line indicate the fitting by Jonscher's power law). (b) Variation of exponent n versus temperature. The decrease in n with increasing temperature suggests the correlated barrier hopping (CBH) mechanism for conduction.

where σ_{ac} is the total conductivity; σ_{dc} is the extrapolated dc conductivity; A is material specific temperature dependent constant, ω is the angular frequency and n ($0 \leq n \leq 1$) is a temperature and frequency dependent exponent.

The $\sigma_{ac}{}'$ extrapolated to lowest measured frequency gives the value of dc conductivity, alternately it can also be found out using Jonscher's power law fitted to experimental data. The value of dc conductivity found to vary between 10^{-12} to 10^{-4} σ/cm for temperature $-30\,°C$ to $330\,°C$, indicating the highly resistive nature of the fine grained, microwave sintered $BiFeO_3$ ceramics; a marked improvement over the conventionally sintered BFO ceramics. Further, the trend of the exponent 'n' gives the nature of the conduction mechanism that may exist in the sample.[45,46] Various models have been developed based on the behavior of n such as QMT (Quantum Tunneling Mechanism, where value of 'n' is independent of temperature), OLPT (Overlapping Large Polaron Tunneling, where n reaches a minimum followed by increases with temperature), and CBH (Correlated Barrier Hopping, where n decreases with temperature).[47] In microwave sintered, fine grained BFO ceramics, the value of n (Figure 6(b)) decreases with temperature which is consistent with the CBH model and is also in agreement to the reported literature.[48]

The activation energy of conduction is obtained by using the Arrhenius plots, $10^3/T$ vs $\sigma_{ac}{}'$ and using the Arrhenius equation,

$$\sigma_{dc} = \sigma_o \exp(-E_a/k_B T) \tag{4}$$

where, σ_o is pre-exponential factor, E_a is activation energy, and k_B is the Boltzmann's constant. From the Arrhenius plots (see Figure 7) two distinct activation energies for microwave sintered BFO ceramics have been observed in the measured temperature range. Solid line indicates the fitted data, from which activation energy was calculated. The activation energy of the conduction was found to be 1.09(±2) eV for > 230 °C, and 0.63 (±2) eV for temperature less than 230 °C.

So far we attributed the occurrence of apparent large $\varepsilon_r{}'$ to the external Maxwell-Wagner response, hopping of charge carriers between the available Fe^{+3} and Fe^{+2} valence states and interfacial/space-charge polarization. However, there have a lot of reports on the applicability of internal barrier layer capacitance (IBLC) effect in few of the oxide ceramics which have shown exceptionally high $\varepsilon_r{}'$ albeit showing high loss.[17,18,21,34,49–53] This IBLC effect arises predominantly due to the heterogeneity in the electrical microstructure of the ceramics. Impedance spectroscopy is a useful tool to study the electrical heterogeneity of the sample, which can be done by deciphering the contribution of the grain and grain boundaries. To decipher the contributions of grains and grain boundaries in microwave sintered, fine grained BFO ceramics we have used the complex impedance plots (Z′ vs Z″). The complex impedance spectrum at a few discrete temperatures is shown in Figure 8.

The figure shows the depressed semicircles, which indicated the distribution in relaxation times. The relaxation in the spectrum can be represented by an equivalent parallel RC circuit, as
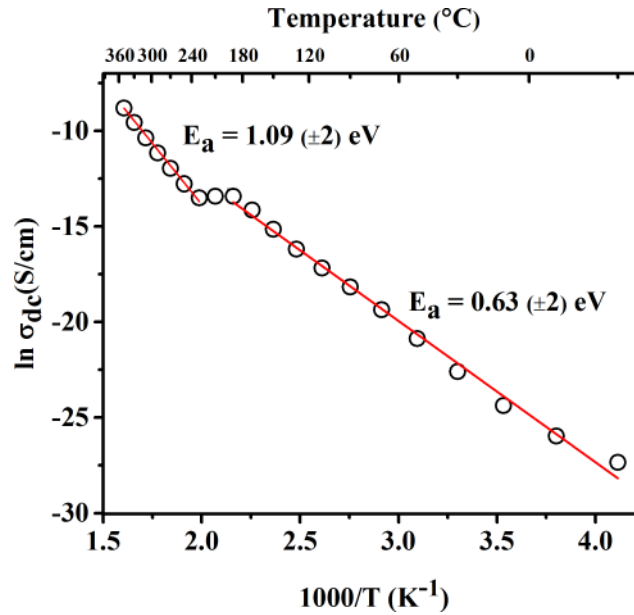
FIG. 7. DC conductivity (σ_{dc}) versus 1000/T plot to find an activation energy of BFO sample (E_a: activation energy calculated from the slope). Two different activation energy can be seen for two different temperature regions.

there are two or more relaxation times, a combination of parallel RC circuit can be used, each representing contribution/relaxation times of grain, grain boundary *etc*. Here the dotted line represents the measured data, and red line indicates fitted data by equivalent parallel RC circuit model. The measured data is fitted by using two parallel RC circuit model. The equivalent circuit model is shown in the inset of Figure 8(a). Each RC element represents the contribution of grains and grain boundaries and electrode effect.[54] The low frequency response is from grain boundary and electrode effect while the high-frequency response corresponds to the grain (bulk). The variation of impedance can be understood by the equivalent circuit and fit according to the following equations,

$$Z' = \frac{R_g}{1 + (\omega R_g C_g)^2} + \frac{R_{gb}}{1 + (\omega R_{gb} C_{gb})^2} \tag{5}$$

$$Z'' = R_g \left[\frac{\omega R_g C_g}{1 + (\omega R_g C_g)^2} \right] + R_{gb} \left[\frac{\omega R_{gb} C_{gb}}{1 + (\omega R_{gb} C_{gb})^2} \right] \tag{6}$$
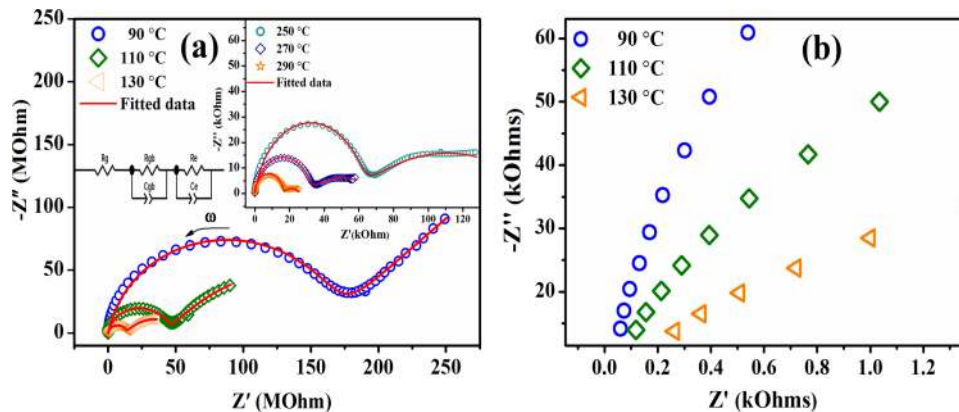

FIG. 8. (a) Variation of Z' versus Z'' (Nyquist plot) for BFO sample at different temperatures. The data is fitted to two equivalent parallel RC circuits, the schematic of which is shown in the inset. (b) Amplification of Nyquist plot for estimation of grain resistance exhibiting.

where, R_g and R_{gb} are grain and grain boundary resistances while, C_g and C_{gb} are capacitances of grain and grain boundaries respectively. The temperature has a profound effect on the conductivity *vis-a-vis* impedance behavior as it is observed that with the temperature concentration of Bi^{2+} cations increase according to the following defect reaction,

$$O_o \Leftrightarrow V_o + \frac{1}{2}O_2 \tag{7}$$

$$V_o \Leftrightarrow V_o^{\infty} + 2e' \tag{8}$$

$$Fe^{3+}(Bi^{3+}) + e' \Leftrightarrow Fe^{2+}(Bi^{2+}) \tag{9}$$

This will create a higher level of electron hopping in samples resulting in a large capacitance for the grain that cannot be ignored, as compared to the capacitance of the grain boundaries.

Figure 9 depicts the variation of R_g, R_{gb}, C_g and C_{gb} with temperature obtained by fitting the complex impedance plots. It can be clearly seen from Figure 9(a) that R_g has resistance in the range from 5 to 200 Ohms in the measured temperature range. While values of R_{gb} was found in the order of 10^9 Ω-cm at room temperature which decreases to 10^3 Ω-cm at 350 °C R_{gb}. The values of R_g and R_{gb} clearly reveal the electrical heterogenity of the microwave sintered BFO, with semicondcuting grains and insulating grain boundaries. Further, the capacitance values of capacitance estimated from the modulus spectra, C_g and C_{gb}, are plotted in Figure 8(b) as a function of temperature. The C_g was found to be of the order of 10^{-11} F, corresponding to the bulk capacitance, and almost remains independent of the measured temperature range. The values of C_{gb} can be seen to vary in range from 10^{-10} F to 10^{-5} F, which correspond to the grain boundary capacitance, and is seen strongly temperature dependent. The activation energies of grain and grain boundaries are calculated by plotting a conductivity versus 1000/T. It is observed from Figure 9(c) that activation
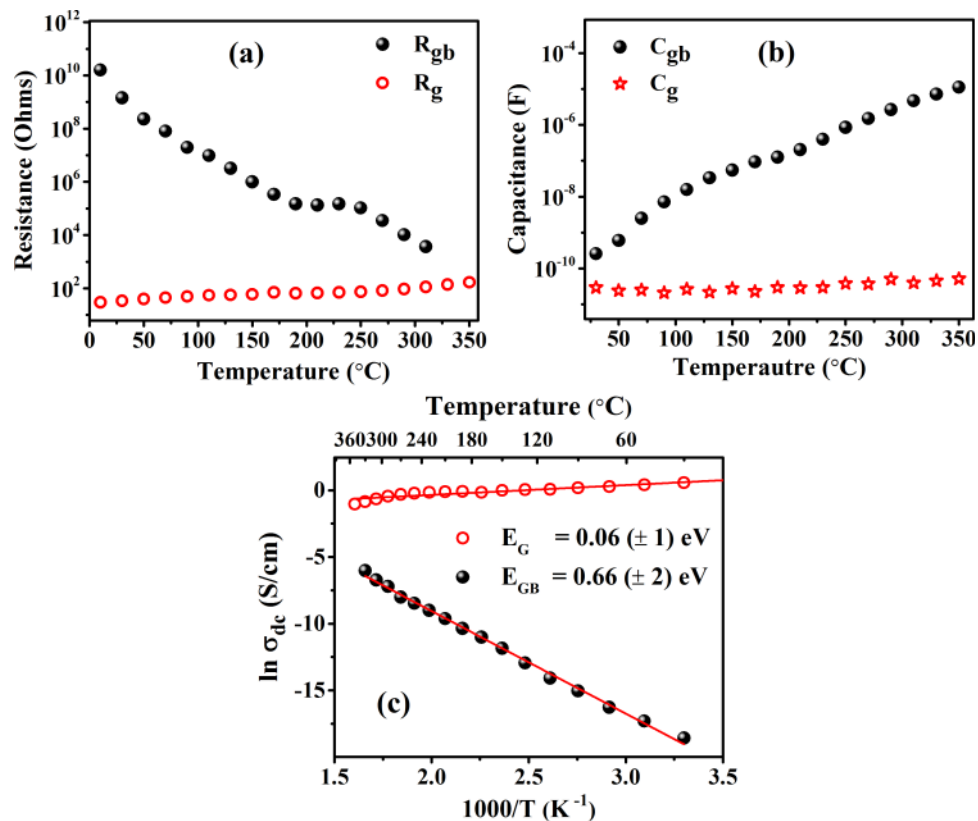

FIG. 9. (a) Variation of grain (R_g) and grain boundary resistance (R_{gb}) with temperature (b) grain (C_g) and grain boundary (C_{gb}) capacitance with temperature and (c) grain (E_g) and grain boundary (E_{gb}) activation energies using dc conductivity values obtained from fitting Nyquist plots.
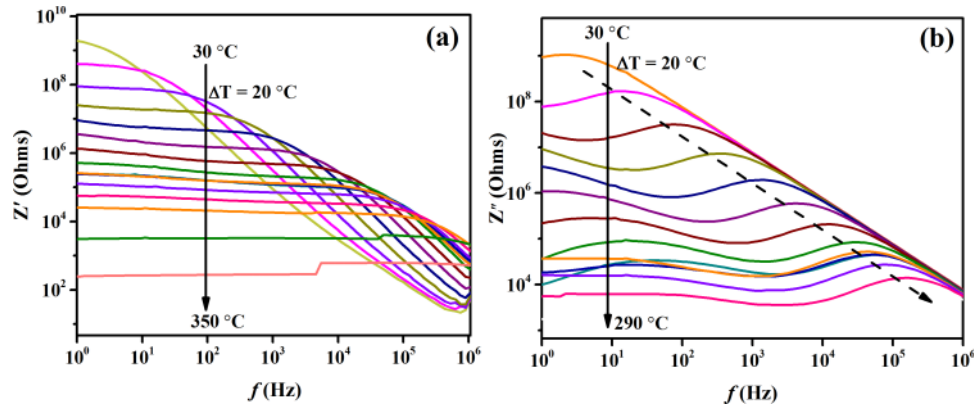
FIG. 10. Frequency dependent (a) real part (Z') and (b) imaginary part (Z'') of impedance of BFO sample measured at different temperatures. Two distinct peaks in Z'' clearly indicates grain and grain boundary contribution.

energy of grain is 0.06 eV. Activation energy of Grain boundary is 0.63 eV and corresponds to p type hopping mechanism.[55]

Further, to gain insight of the conduction process complex impedance study ($Z = Z' - jZ''$) have been performed at different temperatures (see Figure 10). It is clear from the graph that for low temperatures (< 100 °C) Z' decreases monotonically with the frequency (Figure 10(a)) indicate the increase in AC conductivity. Here the slope of Z' versus frequency shows capacitor characteristics (linear) with slope approximately equal to −1. The Z' decreases with the temperature, which suggests some contribution from space charge species. The peaks in Figure 10(b) clearly indicates relaxation in the sample. Two peaks can be observed in the sample. The peak position shift to higher frequency side as the temperature increases (indicated by arrow). The lower frequency peak can be attributed to grain boundary while the peak at high frequency corresponds to the grains.

IV. CONCLUSIONS

Nanocrystalline fine grained $BiFeO_3$ ceramics were successfully synthesized in phase pure form by using Sol gel method followed microwave sintering. Microwave sintering has significantly reduced the sintering temperature and time. Further, this microwave sintered fine grained ceramics were highly dense and insulating (R ~ 1.8 GΩ. cm). Electrical microstructure was probed by complex impedance study and has clear evidences for electrical heterogeneity in the sample. Impedance study reveals semiconducting grains and insulating grain boundaries. We propose, this network of insulating grain boundaries and semiconducting grains could lead to IBLC effect in the sample attributing towards high dielectric constant, along with other extrinsic effects.

[1] G. Catalan and J. F. Scott, Adv. Mater. **21**, 2463 (2009).
[2] M. Polomska, W. Kaczmarek, and Z. Pająk, Phys. Status Solidi A **23**, 567 (1974).
[3] F. Kubel and H. Schmid, Acta Crystallogr B **46**, 698 (1990).
[4] W. Eerenstein, N. D. Mathur, and J. F. Scott, Nature **442**, 759 (2006).
[5] S. Y. Yang, L. W. Martin, S. J. Byrnes, T. E. Conry, S. R. Basu, D. Paran, L. Reichertz, J. Ihlefeld, C. Adamo, A. Melville, Y.-H. Chu, C.-H. Yang, J. L. Musfeldt, D. G. Schlom, J. W. Ager, and R. Ramesh, Appl. Phys. Lett. **95** (2009).
[6] J. Wang, J. B. Neaton, H. Zheng, V. Nagarajan, S. B. Ogale, B. Liu, D. Viehland, V. Vaithyanathan, D. G. Schlom, U. V. Waghmare, N. A. Spaldin, K. M. Rabe, M. Wuttig, and R. Ramesh, Science **299**, 1719 (2003).
[7] S. H. Baek, H. W. Jang, C. M. Folkman, Y. L. Li, B. Winchester, J. X. Zhang, Q. He, Y. H. Chu, C. T. Nelson, M. S. Rzchowski, X. Q. Pan, R. Ramesh, L. Q. Chen, and C. B. Eom, Nat Mater **9**, 309 (2010).
[8] S. M. Selbach, M.-A. Einarsrud, and T. Grande, Chem. Mater. **21**, 169 (2008).
[9] T. Rojac, M. Kosec, B. Budic, N. Setter, and D. Damjanovic, J. Appl. Phys. **108** (2010).

[10] T. Rojac, M. Kosec, and D. Damjanovic, J. Am. Ceram. Soc. **94**, 4108 (2011).
[11] J. Silva, A. Reyes, H. Esparza, H. Camacho, and L. Fuentes, Integr Ferroelectr **126**, 47 (2011).
[12] X. Qi, P.-C. Tsai, Y.-C. Chen, Q.-R. Lin, J.-C.-A. Huang, W.-C. Chang, and I.-G. Chen, Thin Solid Films **517**, 5862 (2009).
[13] H. Béa, M. Bibes, A. Barthélémy, K. Bouzehouane, E. Jacquet, A. Khodan, J.-P. Contour, S. Fusil, F. Wyczisk, A. Forget, D. Lebeugle, D. Colson, and M. Viret, Appl. Phys. Lett. **87** (2005).
[14] T. Liu, Y. Xu, and J. Zhao, J. Am. Ceram. Soc. **93**, 3637 (2010).
[15] Y.-H. Lin, M. Li, C.-W. Nan, J. Li, J. Wu, and J. He, Appl. Phys. Lett. **89**, 032907 (2006).
[16] R. Waser and R. Hagenbeck, Acta Mater. **48**, 797 (2000).
[17] P. Thongbai, C. Masingboon, S. Maensiri, T. Yamwong, S. Wongsaenmai, and R. Yimnirun, J. Phys.: Condens. Matter **19**, 236208 (2007).
[18] S. Maensiri, P. Thongbai, and T. Yamwong, Appl. Phys. Lett. **90**, 202908 (2007).
[19] C. Masingboon, S. Maensiri, T. Yamwong, P. L. Anderson, and S. Seraphin, Appl. Phys. A **91**, 87 (2007).
[20] C. Masingboon, P. Thongbai, S. Maensiri, T. Yamwong, and S. Seraphin, Mater. Chem. Phys. **109**, 262 (2008).
[21] D. C. Sinclair, T. B. Adams, F. D. Morrison, and A. R. West, Appl. Phys. Lett. **80**, 2153 (2002).
[22] M. C. Ferrarelli, T. B. Adams, A. Feteira, D. C. Sinclair, and A. R. West, Appl. Phys. Lett. **89**, 212904 (2006).
[23] W. Cai, C. Fu, G. Chen, X. Deng, K. Liu, and R. Gao, J. Mater. Sci. - Mater. Electron. **25**, 4841 (2014).
[24] A. Mahapatra, S. Parida, S. Sarangi, and T. Badapanda, JOM (2014).
[25] W. Cai, C. Fu, W. Hu, G. Chen, and X. Deng, J. Alloys Compd. **554**, 64 (2013).
[26] S. Katlakunta, P. Raju, S. S. Meena, S. Srinath, R. Sandhya, P. Kuruva, and S. R. Murthy, Physica B Condens Matter **448**, 323 (2014).
[27] S. Mohammadi, H. Shokrollahi, and M. H. Basiri, J. Magn. Magn. Mater. **375**, 38 (2015).
[28] V. Raghavendra Reddy, D. Kothari, S. Kumar Upadhyay, A. Gupta, N. Chauhan, and A. M. Awasthi, Ceram. Int. **40**, 4247 (2014).
[29] S. Mahajan, O. P. Thakur, D. K. Bhattacharya, and K. Sreenivas, J. Am. Ceram. Soc. **92**, 416 (2009).
[30] J. Rodríguez-Carvajal, Physica B Condens Matter **192**, 55 (1993).
[31] T. Rojac, A. Bencan, B. Malic, G. Tutuncu, J. L. Jones, J. E. Daniels, and D. Damjanovic, J. Am. Ceram. Soc. **97**, 1993 (2014).
[32] S. H. Song, Q. S. Zhu, L. Q. Weng, and V. R. Mudinepalli, J. Eur. Ceram. Soc. **35**, 131 (2015).
[33] S. Hunpratub, P. Thongbai, T. Yamwong, R. Yimnirun, and S. Maensiri, Appl. Phys. Lett. **94**, 062904 (2009).
[34] J. W. Chen, J. C. Wang, and Y. F. Chen, Physica C Supercond **289**, 131 (1997).
[35] F. Kremer and A. Schonhals, *Broadband Dielectric Spectroscopy* (Springer, Berlin Heidelberg, 2003).
[36] C. C. Wang, Y. M. Cui, G. L. Xie, C. P. Chen, and L. W. Zhang, Phys. Rev. B **72**, 064513 (2005).
[37] R. K. Mishra, D. K. Pradhan, R. N. P. Choudhary, and A. Banerjee, J. Phys.: Condens. Matter **20**, 045218 (2008).
[38] A. Gautam, K. Singh, K. Sen, R. K. Kotnala, and M. Singh, J. Alloys Compd. **517**, 87 (2012).
[39] S. Ke, P. Lin, X. Zeng, H. Huang, L. M. Zhou, and Y. W. Mai, Ceram. Int. **40**, 5263 (2014).
[40] A. K. Pradhan, K. Zhang, D. Hunter, J. B. Dadson, G. B. Loiutts, P. Bhattacharya, R. Katiyar, J. Zhang, D. J. Sellmyer, U. N. Roy, Y. Cui, and A. Burger, J. Appl. Phys. **97**, 093903 (2005).
[41] Q.-h. Jiang, C.-w. Nan, Y. Wang, Y.-h. Liu, and Z.-j. Shen, J. Electroceram. **21**, 690 (2008).
[42] S. Vijayanand, H. S. Potdar, and P. A. Joy, Appl. Phys. Lett. **94**, 182507 (2009).
[43] K. S. Cole and R. H. Cole, J Chem Phys **9**, 341 (1941).
[44] A. K. Jonscher, Nature **267**, 673 (1977).
[45] S. Kabi and A. Ghosh, J. Appl. Phys. **107**, 103715 (2010).
[46] A. Singh, R. Chatterjee, S. K. Mishra, P. S. R. Krishna, and S. L. Chaplot, J. Appl. Phys. **111**, 014113 (2012).
[47] A. Ghosh, Phys. Rev. B **42**, 1388 (1990).
[48] D. Rajasree, S. Tanushree, and K. Mandal, J. Phys. D: Appl. Phys. **45**, 455002 (2012).
[49] H. Wu, Y. B. Lin, J. J. Gong, F. Zhang, M. Zeng, M. H. Qin, Z. Zhang, Q. Ru, Z. W. Liu, X. S. Gao, and J. M. Liu, J. Phys. D: Appl. Phys. **46**, 145001 (2013).
[50] P. Salame, R. Drai, O. Prakash, and A. Kulkarni, Ceram. Int. **40**, 4491 (2013).
[51] P. Salame, O. Prakash, and A. Kulkarni, J. Am. Ceram. Soc. **96**, 2184 (2013).
[52] S. I. R. Costa, M. Li, J. R. Frade, and D. C. Sinclair, RSC Adv **3**, 7030 (2013).
[53] T. B. Adams, D. C. Sinclair, and A. R. West, Phys. Rev. B **73**, 094124 (2006).
[54] J. T. S. Irvine, D. C. Sinclair, and A. R. West, Adv. Mater. **2**, 132 (1990).
[55] A. Makhdoom, M. Akhtar, R. Khan, M. Rafiq, M. Hasan, F. Sher, and A. Fitch, Mater. Chem. Phys. **143**, 256 (2013).